VERIFICATION AND VALIDATION OF LAMINAR NAVIER-STOKES APPLICATIONS

Bruno Goffert, bruno_goffert@hotmail.com
Instituto Tecnológico de Aeronáutica (ITA), Pça. Marechal Eduardo Gomes, 50, São José dos Campos – SP, CEP: 12.228-901

Maycol Marcondes Vargas, myl_vargas@hotmail.com
Universidade de Taubaté, Rua Daniel Danelli s/n, Jardim Morumbi, Taubaté – SP, CEP: 12060-440,

João Batista Pessoa Falcão Filho, jb.falcao@ig.com.br
Instituto de Aeronáutica e Espaço (IAE), Divisão de Aerodinâmica (ALA), Pça. Marechal Eduardo Gomes, 50
CEP: 12228-904 , São José dos Campos, São Paulo

Abstract. *The use of CFD codes has had a progressive participation in aeronautical research. In particular its application to analyze confined flows like those present in wind tunnels has supported physical phenomena investigations. With this motivation, it is being developed in the Aerodynamic Division (ALA) of the Institute of Aeronautics and Space (IAE) a numerical code in order to simulate the flow over models installed in the test section of the Pilot Transonic Wind Tunnel (PTT) of IAE. In a first attempt, the code will be used to simulate a NACA 0012 profile to help understanding the physical phenomena involved during the experimental tests proposed in PTT in the transonic regime (from Mach number 0.60 to 1.00), and to suggest corrections for the compressibility and wall effects for the experimental data obtained. This work describes the progress in the code development with the inclusion of viscous terms. The new code version was subjected to verification and validation procedures to guarantee its reliability in some applications. Five different physical situations were selected from different classes of laminar flows: incompressible free boundary-layer, compressible free boundary-layer, interference of shock-wave on boundary-layer, incompressible flow between flat plates and flow in a supersonic convergent-divergent nozzle. These cases represent classical problems for which a lot of results can be found.*

Keywords*: CFD code, laminar flow, boundary layer, convergent-divergent nozzle, verification and validation*

1. INTRODUCTION

It is a need today the use of numerical results from CFD (Computational Fluid Dynamics) to help in aeronautical research, optimizing experimental tests to reduce time and cost. One very impressive example comes from EMBRAER ("Empresa Brasileira de Aeronáutica"), the Brazilian airplane manufacturer, which has shown a natural evolution in the use of CFD techniques through all the 35 years of project developments (Resende, 2004). Beginning with the EMB-110 Bandeirante (which actually began its development as the IPD/PAR 6504 project at CTA – "Centro Técnico Aeroespacial" in São José dos Campos), the use of empirical methods was very common during theoretical investigation. With the EMB-120 Brasília, a two-dimensional panel method was used to improve root profile CL_{max} characteristics. And, passing through a continuous project evolution together with computational simulations and wind tunnel experimental results, it is possible to observe a strong CFD participation in the designs. This fact is more evident in the jet family Embraer 170, in which many specific methods were developed in each part of the aircraft: the Euler multi-component methodology with boundary-layer influence correction for analysis and design of the transonic profile configuration, three-dimensional potential method for the analysis of the wing, three-dimensional panel methods for pilon/nacele, slat, and flaps designs, and three-dimensional Euler/Navier-Stokes method for analysis of wing-pilon-nacele assembly, and for winglet design.

It is also very important to observe the application of CFD to analyze confined flows like those present in wind tunnels, as they were used to support physical phenomena investigations. Murman (1972) presented a method for determining the interference effects due to test section walls on the transonic profile lift characteristics, applied to NACA 0012 profile. König *et al.* (2008) studied the drag reduction due to control bumps over profile in tests performed in the Göttingen wind tunnel and from numerical simulations of the same situations, in order to determine the wall influence on the control bumps performance.

With the same motivation in mind, it is being developed in the Aerodynamic Division (ALA) of the Institute of Aeronautics and Space (IAE) a numerical code in order to simulate the flow over models installed in the test section of the Pilot Transonic Wind Tunnel (PTT) of IAE. In a first attempt, the code will be used to simulate a NACA 0012 profile. The main objective is to help understanding the physical phenomena involved during the experimental tests proposed in PTT in the transonic regime (from Mach number 0.60 to 1.00), and to suggest corrections for the compressibility and wall effects for the experimental data obtained.

The numerical code, originally based on the Beam and Warming centered finite-difference method, was developed to solve the Euler equations, and it was applied to the flow over a NACA 0012 profile (Goffert and Falcão Filho, 2009). The present work represents the next natural step in the code development, with the inclusion of the viscous terms. This

work shows the code main characteristics and five well-known problems of physical interests, which were selected in order to apply the verification and validation procedures (Oberkampf and Trucano, 2002, Eça *et al.*, 2007).

2. MATHEMATICAL MODELING

It is common recognize the collection of the continuity, momentum, energy, and any constitutive equation necessary to represent the fluid medium by "Navier-Stokes equations". They may be written in two-dimensional generalized body-conforming coordinates, and in conservation-law form by (Anderson *et al.*, 1984)

$$\frac{\partial \overline{Q}}{\partial \tau}+\frac{\partial \overline{E}}{\partial \xi}+\frac{\partial \overline{F}}{\partial \eta}=0\,, \tag{1}$$

and, the variable-conserved vector is given by

$$\overline{Q}=J^{-1}\left[\rho \quad \rho u \quad \rho v \quad e\right], \tag{2}$$

where ρ is density, u and v are velocity Cartesians coordinates and e is total energy.

The flux vectors, for fixed grid, are

$$\overline{E}=\frac{1}{J}\begin{bmatrix}\rho U\\ \rho u U+p\xi_x\\ \rho v U+p\xi_y\\ (e+p)U\end{bmatrix}-\frac{1}{J\,Re}\begin{bmatrix}0\\ \tau_{xx}\xi_x+\tau_{xy}\xi_y\\ \tau_{xy}\xi_x+\tau_{yy}\xi_y\\ \beta_x\xi_x+\beta_y\xi_y\end{bmatrix}, \tag{3}$$

$$\overline{F}=\frac{1}{J}\begin{bmatrix}\rho V\\ \rho u V+p\eta_x\\ \rho v V+p\eta_y\\ (e+p)V\end{bmatrix}-\frac{1}{J\,Re}\begin{bmatrix}0\\ \tau_{xx}\eta_x+\tau_{xy}\eta_y\\ \tau_{xy}\eta_x+\tau_{yy}\eta_y\\ \beta_x\eta_x+\beta_y\eta_y\end{bmatrix}, \tag{4}$$

where p is the pressure. Adopting the perfect gas hypotheses, p may be expressed by

$$p=\rho(\gamma-1)\left[\frac{e}{\rho}-\frac{1}{2}(u^2+v^2)\right]. \tag{5}$$

Re is the Reynolds number given by

$$Re=\frac{\rho_R V_R \ell}{\mu_R}, \tag{6}$$

where ρ_R, V_R, ℓ and μ_R are referenced values of density, velocity, length and dynamic viscosity, respectively.

The curvilinear coordinate system is defined such as ξ is the stream-wise direction, represented by the computational direction i, and η is the transversal-wise direction, represented by the computational direction j. This coordinate system is obtained from the Cartesian system (x, y) through the relations:

$$\tau=t\,, \tag{7}$$

$$\xi=\xi(t,x,y)\,, \tag{8}$$

$$\eta=\eta(t,x,y)\,, \tag{9}$$

and the transformation jacobian is given by

$$J=\left(x_\xi y_\eta-x_\eta y_\xi\right)^{-1}. \tag{10}$$

The contra-variant velocity components are defined as:

$$U = \xi_t + \xi_x u + \xi_y v\,, \tag{11}$$

$$V = \eta_t + \eta_x u + \eta_y v\,. \tag{12}$$

Definitions of the terms β_x, β_y, τ_{xx}, τ_{yy}, τ_{xy} may be found in Falcão Filho and Ortega (2008).

The code used was originated in the implicit approximate factorization finite difference algorithm proposed by Beam and Warming (1978), for which the space derivatives are approximated using centered schemes, and the time marching is undertaken through implicit Euler method. To simplify the numerical code and consequently to reduce computational cost, the code was adapted to follow the diagonal algorithm of Pulliam and Chaussee (1981) complemented by a non-linear, spectral-radius-based artificial dissipation strategy due to Pulliam (1986). This implementation maintains the whole stability characteristics and accuracy for steady-state applications (Falcão Filho, 2006). Normally centered schemes are stable only with the use of artificial dissipation and this combination leads to difficulties in capturing flow discontinuities, like shock waves. The use of simple schemes results in passages through shocks not so well defined, as for example, those oscillations that occur in the pre-shock and post-shock regions (Pulliam, 1986). So, a more sophisticated, non-linear, spectral-radius-based artificial dissipation strategy was implemented to the code (Pulliam, 1986, Mello, 1994, Falcão Filho, 2006). The artificial dissipation scheme is fourth-order but through high pressure gradients, like those present in shock wave passages, the scheme is altered to a second-order. In this way, the shock passage can be well captured like those obtained with upwind schemes. All numerical details about the code implementation may be found in Falcão Filho and Ortega (2008).

2. VERIFICATION AND VALIDATION PROCEDURES

When in most flows of practical engineering interest there are no analytical solutions for the Navier-Stokes equations, CFD is an established alternative. However, the ability to produce a numerical solution is not enough. The credibility of CFD as an Engineering tool depends on the quantification of the error/uncertainty of the results.

During the last four decades verification and validation procedures applied to CFD codes have been passed by successive improvements. The great gain has been related to a better understanding of them and a precise distinction between verification, which guarantees that the equations are being correctly solved, and validation, which guarantees that the corrected equations for the physical problem are being solved. A noticeable work of Oberkampf and Trucano (2002) shows how to determine the order of the method, and describes some of the first important works developed until that time. More recently, the ASME (2008), American Society of Mechanical Engineering, has prepared a guide to apply the verification and validation procedures. The idea that it is not possible to have a numerical code verified and validated to a large class of problems is something relatively new in the scientific community, which realizes the need of getting numerical results that may prove the quality of the obtained solutions, for a given precision, in each particular problem (Eça *et al.*, 2007).

2.1. Verification

Verification tries to check if spatial discretization is sufficient, if temporal (in transient problems) is sufficient, if the loop procedure has converged, if the round-off error is sufficiently low and if there are errors in the code language.

Some procedures for the verification of the code applied to five well known physical situations are presented to determine the order of the method and analyze the mesh refinement. The determination of the numerical solution order of the method is fundamental to obtain data reliability. It is possible to calculate the order of the method by comparing the errors obtained between each one of two simulations (with different mesh refinements) with an analytical solution ("exact solution"). When the analytical solution is not available, it is possible to use a numerical solution with a great and sufficient refinement.

For each mesh, with grid displacement given by h, it is calculated its error $err(h)$ for many points in the calculation domain, using the expression:

$$err(h) = \left| \, exact\ value - obtained\ numerical\ value \, \right|. \tag{13}$$

With the relative errors related to two meshes with different refinements, h_1 and h_2, the expression that gives the order of the method is given by (Oberkampf and Trucano, 2002):

$$O = \frac{log\left[\frac{err\,(h_1)}{err\,(h_2)}\right]}{log\left[\frac{h_1}{h_2}\right]}. \tag{14}$$

Since the adopted method is of spatial order of precision 2, that means that, if the mesh refinement causes the displacement to decrease to the half, consequently the errors in the same calculation positions will be reduced four times.

Another verification procedure deals with the adequacy of the mesh refinement adopted. Or, does the discrete solution converge to the exact solution as the mesh spacing is reduced in real calculations? This fact may be checked by comparing successive mesh refinement solutions related to a chosen flow parameter distribution. As the mesh is refined the solution tends to an asymptotic solution. The plotting of the solutions gives a better understanding of this fact.

2.2. Validation

Practically the validation procedures deals with the determination of the numerical solutions compared with confident experimental data. Some guidelines should be observed during the code development concerning validation. Among them, two are very important. First, a validation experiment should be jointly designed by experimentalists, model developers, code developers, and code users, working closely together throughout the program, with open mind about the strengths and weaknesses of each approach adopted. Second, a validation experiment should be designed to capture the essential physics of interest, including all relevant physical modeling data and initial and boundary conditions required by the code.

2.3. Selected Cases

Five different physical situations were selected to verify and validate the code in different classes of problems. These cases represent classical problems for which a lot of results can be found. Table 1 summarizes these cases with the main related flow parameters. Because of lack of space, only the most important results will be presented for each case.

Table 1. Five laminar physical study cases for verification and validation procedures.

case	physical problem	reference	main characteristics
1	incompressible BL (Blasius solution)	Schlichting (1978)	flow velocity 6.8 m/s, Reynolds number 1400
2	compressible BL	Schlichting (1978)	Mach number 2.00, Reynolds number 296,000
3	shock-wave over compressible BL	Hakkinen *et al.* (1959)	Mach number 2.00, Reynolds number 296,000
4	Poiseuille flow	Schlichting (1978)	flow velocity of 6.8 m/s, Reynolds number 156.5
5	convergent-divergent nozzle	Falcão Filho *et al.* (2000)	exit Mach number 1.27, Reynolds number 4250

2.4. Initial and boundary conditions

In all cases, the initial conditions for all mesh points have been established by the non-disturbing flow values at the entrance. This way the total computational time diminishes.

Boundary conditions were established for each case according to their peculiarities. In general, for all solid frontiers the non-slip condition was established to allow the laminar boundary-layer representation. The inlet conditions were in all cases imposed, although in subsonic cases this would not be physically precise. The CFD experience has shown that the possible discrepancy due to imposing all conditions at the inlet plane is negligible in many cases. This way, a more complex to implement scheme was avoided, as the one based on Euler characteristic equations, simplifying the code development. The same fact occurs in the outlet conditions. The zeroth-order extrapolation was applied in all cases, even though only for supersonic flows this is physically corrected. For boundary-layer problems, an outer frontier distance analysis was performed to guarantee that it had no influence over the boundary-layer development.

Other particular details will be described along with the presentation of the results for each case.

3. STUDY CASES – RESULTS

The code was used to solve the classical problems presented in Table 1 with the aim of verifying and validating it, as they test the code in the classes of problems more related with its future use. However, some applications refer to situations very far from a real interest case. For example, to ensure a laminar flow regime the geometric scale of the problem was much reduced. For each test case the following sub-items present the most significant results.

3.1. Incompressible laminar boundary layer (Blasius solution)

Incompressible laminar flow over a flat plate is a fundamental problem in Fluid Mechanics. The boundary-layer is defined as the layer between the zero velocity (non-slip condition) at the flat plate wall to full magnitude at some distance from it. The problem of a laminar flow along a flat plate is the simplest example of the application of the Navier-Stokes equations. It was discussed by Blasius in his memorable doctoral thesis at Goettingen in 1908 and historically it represents the first example illustrating the application of Prandtl´s boundary-layer theory (Schlichting, 1979) – later his work was translated to English (Blasius, 1950). The agreement between theory and experiment is remarkably good. The growth of the boundary layer with increasing distance along the flat plate leads to an unstable situation, and turbulent flow sets in. The laminar regime is observed while the local Reynolds number is kept below 3×10^5. Using velocity profile similar transformation it is possible to obtain the equation

$$f(\eta)\, f''(\eta) + 2\, f'''(\eta) = 0\,, \tag{15}$$

where $f(\eta)$ denotes the dimensionless stream function and η is a dimensionless argument, given by

$$\eta = y\sqrt{\frac{U_0}{\nu\, x}}\,, \tag{16}$$

where x is the distance stream-wise from the flat plate leading edge, y is the distance in perpendicular to the plate direction, U_0 is the free-stream velocity and ν is the local cinematic viscosity. In this approach, $f'(\eta)$ represents the local dimensionless velocity, given by u / U_0 and the boundary conditions for the problem are $f(0) = 0$, $f'(0) = 0$, $f'(\infty) = 1$.

Although being a classical engineering problem, it has called the attention of the scientific community even recently, like the work of Cortell (2005) who addresses it numerically using a Runge-Kutta algorithm for high-order initial value problems.

The study case chosen was that with an undisturbed flow field (Mach number $M_\infty = 0.02$, density $\rho_\infty = 1.00$ kg/m^3, temperature $T_\infty = 287.7$ K) over a flat plate. Figure 1 shows the diagram of the problem with the boundary conditions applied to each particular region. All undisturbed conditions were imposed at the inlet section. All parameters were extrapolated by zeroth-order at the outlet section.

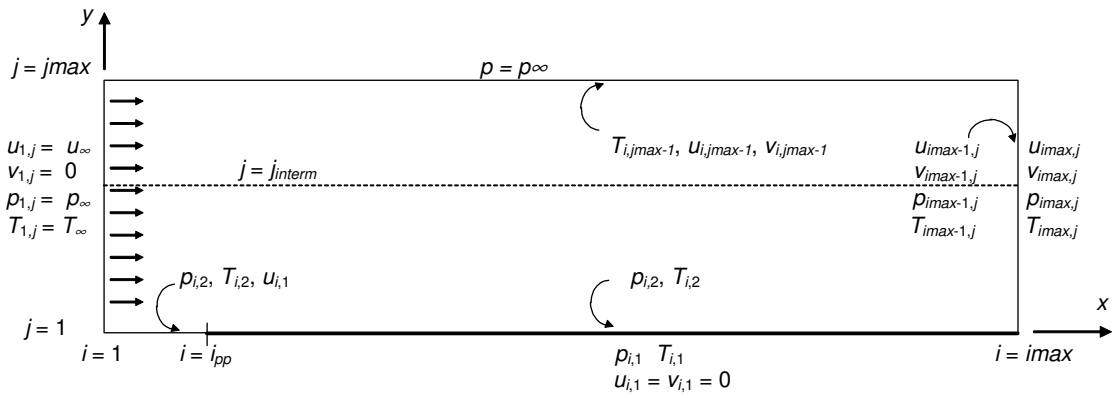

Figure 1. Diagram of incompressible laminar boundary layer over a flat plate (Blasius flow), and boundary conditions.

Figure 2 shows the comparison of the present work with the Blasius solution for the free boundary-layer development over a flat plate, at a local Reynolds number of 1400. The highest error observed was 4 %.

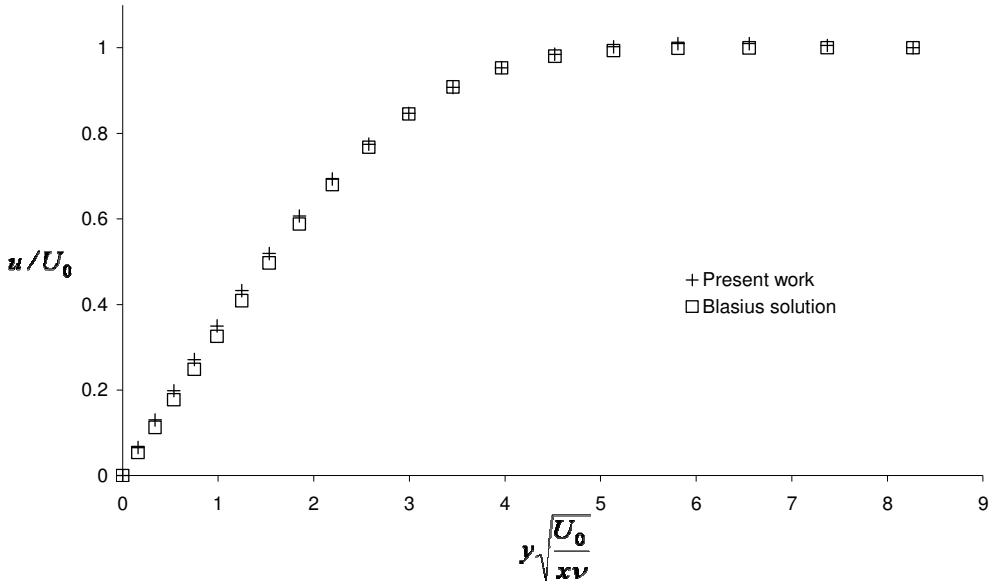

Figure 2. Velocity profile of incompressible laminar boundary-layer over a flat plate (Blasius flow).

3.2. Compressible laminar boundary layer (Mach number 2.0)

When the flow velocity increases the work of compression and energy dissipation in boundary-layer flow produces considerable increases in temperature and the thermal boundary layer must be considered, because the two boundary layers strongly interact each with the other. For a two-dimensional flow there exists a remarkably simple relation between the fields of velocity and temperature. The compressible boundary-layer on a flat plate at zero incidence has been studied extensively in literature and some parameters are worth noting. For example, for adiabatic wall assumption the wall temperature (T_{aw}) can be expressed approximately by

$$T_{aw} = T_\infty \left(1 + \frac{\gamma - 1}{2} \sqrt{Pr}\, M_\infty^{\,2} \right), \tag{17}$$

where T_∞ and M_∞ are temperature and Mach number in the undisturbed flow, and Pr is the Prandtl number, which allows to obtain correlation between flow and temperature boundary layers.

The flow simulated has the following undisturbed parameters: Mach number 2.0, static pressure of 6,156 Pa, static temperature of 162.9 K, which is the same undisturbed condition for the problem studied by Hakkinen (1959) (case 3 in Table 1). Figure 3 shows the results obtained in terms of the velocity (a) and temperature (b) profiles, non-dimensionalized by their free stream values.

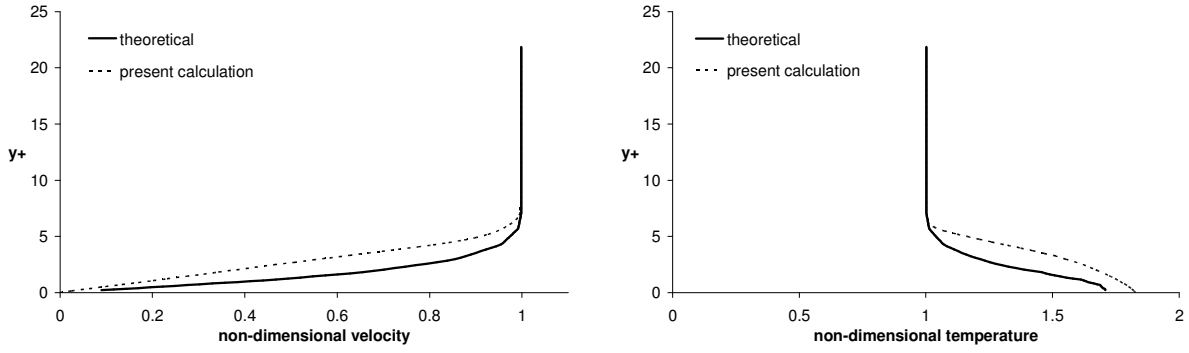

(a) (b)

Figure 3. Velocity (a) and temperature (b) non-dimensional profiles for flow with Mach number 2.0 over a flat plate.

3.3. Shock wave interference over compressible laminar boundary-layer

As it represents a real flight high speed situation, this problem has been addressed for many decades, and new works are still expected when different approaches of comparison between CFD solutions and experiments (Dolling, 2001). Hakkinen *et al.* (1959) made very useful measurements in the laminar boundary layer over a flat plate in which there is an oblique shock wave impinging. This situation was simulated numerically by Beam and Warming (1978) and MacCormack (1981). Both used the same computational mesh, which is also used here. A flat plat is subjected to a high speed flow of free stream Mach number 2.0 aligned to it, while an oblique shock wave with angle 32.6° hits it causing local flow recirculation. Figure 4 shows a diagram of the problem with the boundary conditions applied to each particular region. The free stream flow parameters are determined based on a stagnation pressure of 48.13 kPa, stagnation temperature of 293 K and Mach number 2.0. The after shock parameters are, longitudinal speed 494.5 m/s, transversal speed –26.7 m/s, static pressure 7.127 kPa and static temperature 171.0 K. The shock wave hits the flat plate at 0.049 m from its leading edge, resulting in a local Reynolds number of $Re = 2.96 \times 10^5$.

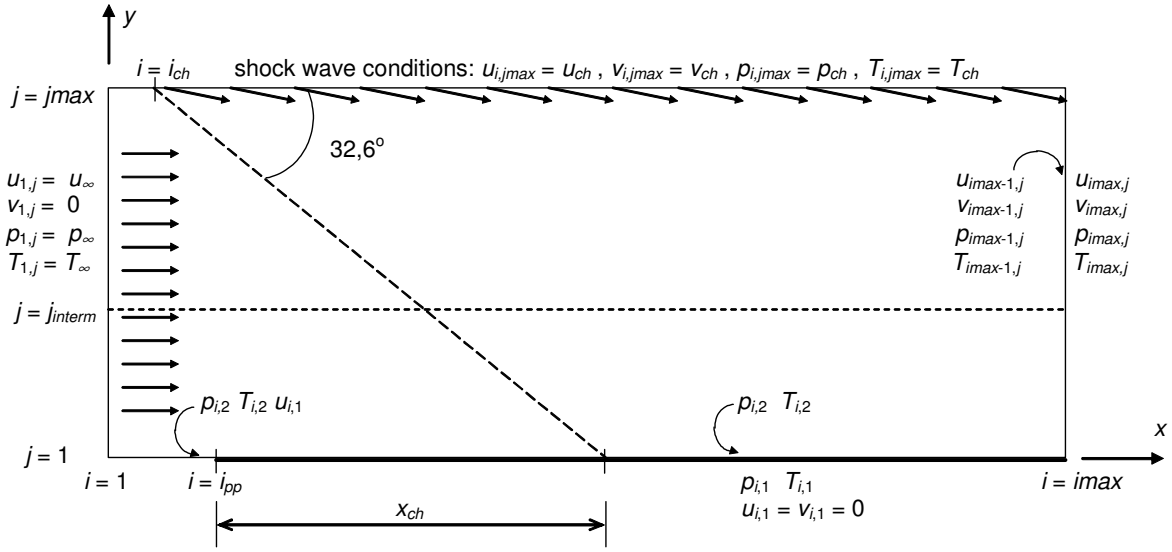

Figure 4. Boundary conditions for the shock wave interference over compressible laminar boundary layer problem.

The numerical calculation showed a good agreement with the experience. Figure 5 (a) shows the pressure distribution in the inferior frontier. There is a pressure increase at the flat plate leading edge ($x = 0.012$ m), caused by a compression wave. In the region of the impinging shock wave the result indicates a pressure increase in two steps due to the recirculation region (see Fig. 5 (b)). The first one when the incident shock wave passage occurs, followed by a small region under the recirculation bubble influence. The second one, after the flow reattachment, caused by the reflected shock wave. Observe that the present numerical results had a better agreement with the experimental, than those other numerical results (Beam and Warming, 1978, MacCormack, 1981).

Figure 6 shows the velocity profiles at the impinging point. The numerical results had a good agreement, although they all have showed a significant disagreement with experimental results. This can be explained by the great difficulty of experimentally measuring the local velocity with a tiny total pressure probe as it was used by Hakkinen (1959), in the presence of a very thin boundary layer and yet with recirculation. Note the absence of negative measurements at the very thin recirculation region.

This particular problem was very helpful during the code developing. The small recirculation region is very susceptible to the artificial dissipation terms influence. So, adjustments in the coefficients were made to ensure that the artificial dissipation influence was lower than the physical effects present, accurately capturing the recirculation region.

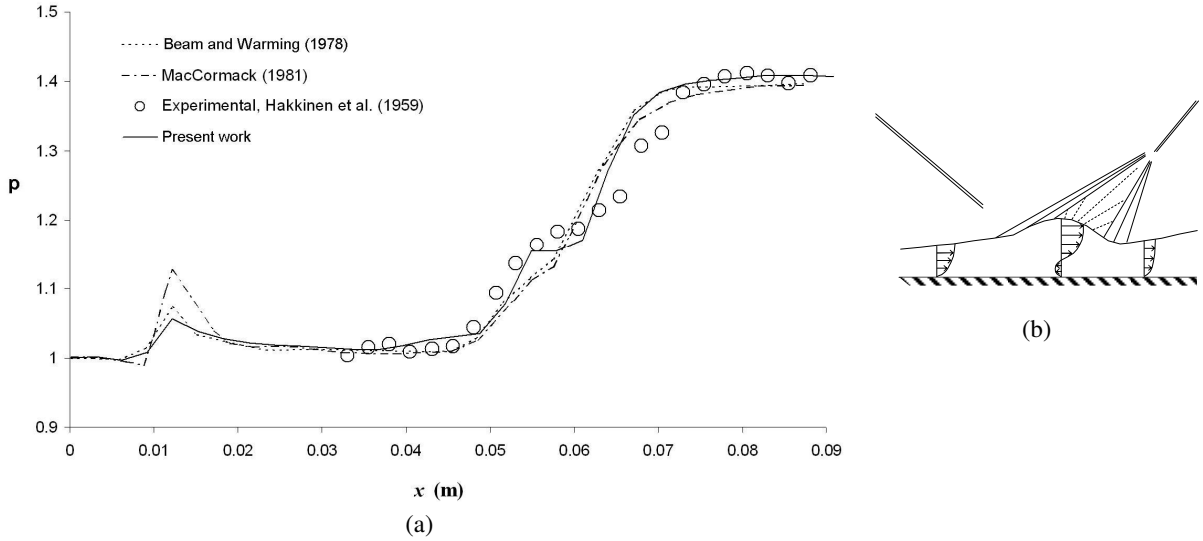

Figure 5. Pressure distribution over inferior frontier non-dimensionalized by inlet static pressure (a), and incident and reflected shock with recirculation region (b).

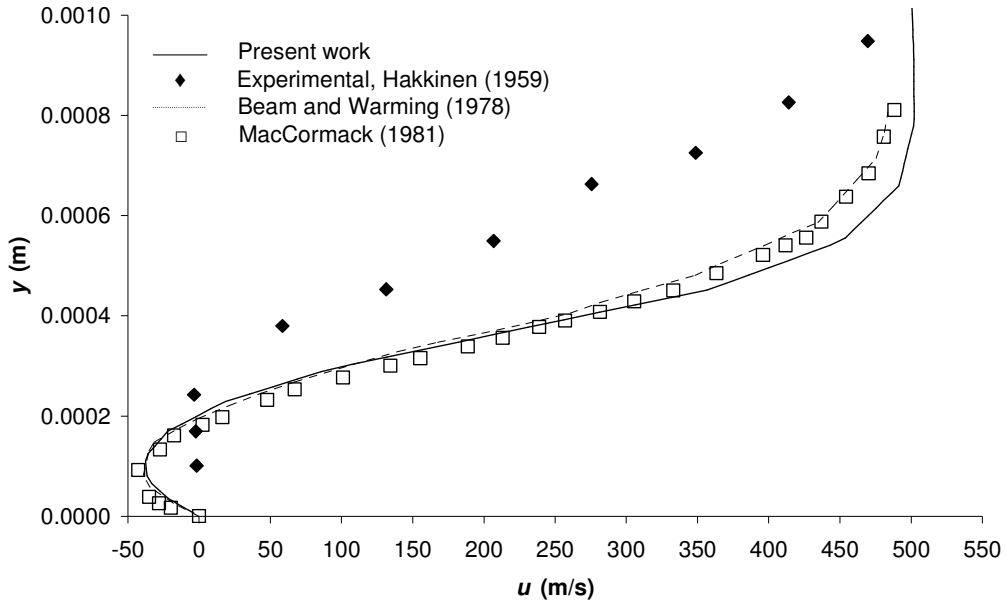

Figure 6. Velocity profile at the shock wave impinging location over the flat plate.

3.4. Laminar flow between plates

The two-dimensional flow between flat and parallel plates are very instructive for many validation procedures. The inlet flow is uniformly distributed over the section height (h) with velocity u_0. The friction process near the walls will form boundary layers which will grow in the streamwise direction until reaching the center of the channel. From this point on, the velocity profile will assume a constant parabolic shape. During the boundary-layer development the flow outside of it feels an area decreasing and tends to accelerate. One can show that the theoretical velocity profile can be expressed by (Schlichting, 1979):

$$u(y) = \frac{3}{2} u_0 \left[1 - \frac{y^2}{\left(h/2\right)^2} \right], \tag{18}$$

where y is the transversal coordinate measured from the center line. For a developed velocity profile the velocity at the center line will be 50% above the velocity at the inlet section. The parabolic profile is formed at about the distance L_D (development length), and it is given by $L_D = 0.04 \cdot h \cdot R_h$, where R_h denotes the Reynolds number referred to the height of the channel (h). For this case, it was chosen the following set of parameters: $u_0 = 6.8$ m/s, $h = 0.004$ m, $R_h = 156.5$, which results in $L_D = 6.3\ h$. The grid was chosen with total length 25 h to guarantee a complete flow development. Four grids with increasing number of points were chose (100×11, 126×13, 158×15 and 200×21) to perform a grid refinement verification.

Figure 7 shows the four velocity profiles obtained with each mesh comparing them with the theoretical solution. With the coarser mesh, the error found was 9.4% and with the finer one, 1.7%. As the refinement increases the relative error diminishes, as expected. Table 2 shows the determination of the order of the method according to Eq. (14). The result shows that the method is about second order of precision. It is worth noting that the code was developed for compressible flow situations and yet it could be used to obtain good results in a very low speed flow (Mach number 0.02). Volpe (1993) has addressed this situation and has showed some of the difficulties that can be encountered. For low speed regimes the density gradients in the field are so low that round-off errors may be important, resulting in bad solutions.

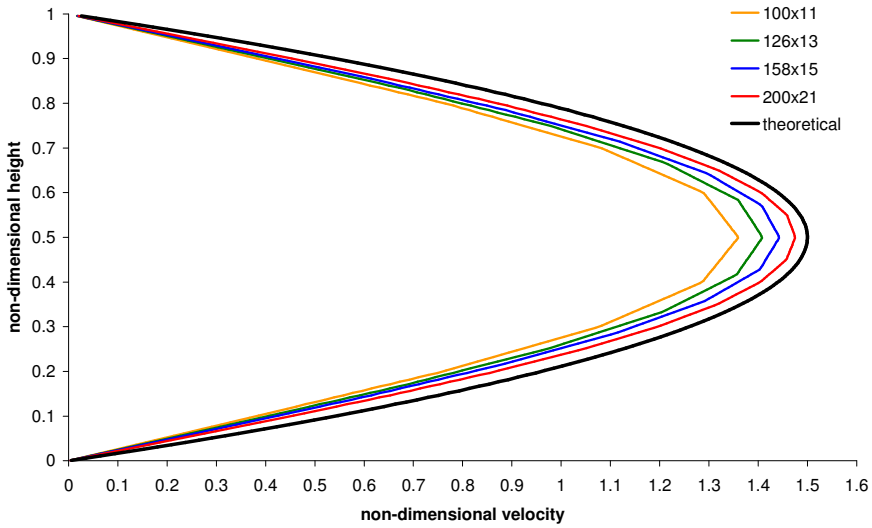

Figure 7. Velocity profiles for the grids used in the simulation, compared with theoretical solution.

Table 2. Calculation of the order of the method.

				Method Order, comparing with		
	h (m)	u_{max}/u_0	err	200x21	158x15	110x11
110x11	0.00091	1.358807	0.141193	2.876107	2.463353	3.126324
126x13	0.00079	1.407666	0.092334	2.802575	2.065149	-
158x15	0.00063	1.442123	0.057877	3.509016	-	-
200x21	0.00050	1.474724	0.025276	-	-	-
theoretical solution	-	1.5	-	-	-	-

3.5. Supersonic convergent-divergent nozzle laminar flow

The geometry considered in this case is a two-dimensional, transonic convergent-divergent nozzle with the throat located half way between the entrance and exit planes (MacCormack, 1985). For viscous flow simulations, the nozzle geometric values, as found in MacCormack work, had to be scaled down 100 times in order to assure laminar regime. The total length of the nozzle is 0.001158 m, the throat height 0.000274 m, the wall radius of curvature at the throat is

0.000274 m and the convergent and divergent angles are 22.33° and 1.21°, respectively. The stagnation temperature, T_0, is equal to 294.8 K while the stagnation pressure, p_0, is 101,360 Pa.

Seven meshes with progressive refinement were used: 21×19, 29×27, 41×38, 59×54, 83×76, 119×107, and 167×152 points. Figure 8 shows the half-nozzle mesh with 59×54 points. As the nozzle geometry is symmetric, only the lower half of the nozzle was considered as the computation domain. All grids were generated algebraically and exponential stretching was implemented for grid refinement near the throat and near the wall, to better account for the shock wave and the boundary-layer, respectively.

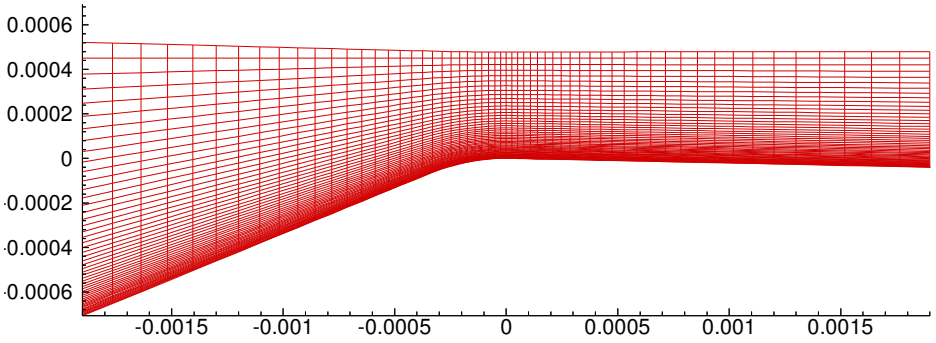

Figure 8. Convergent-divergent grid with 59×54 points.

At the inlet plane, the stagnation pressure and stagnation temperature were imposed. The velocity components were extrapolated by zeroth-order from the inner points. Non-slip conditions were implemented in the lower frontier, with adiabatic wall assumption and boundary-layer presence, by zeroth-order extrapolation of temperature and pressure. It was created one extra line in the upper frontier to extrapolate the symmetrical condition, where pressure, temperature and longitudinal velocity at the last line were made equal to the respective parameters in spectral points related to the symmetrical line. The transversal velocity component was set with the same magnitude and with opposite sign, to reflect the symmetry.

Figure 9 shows the results for the seven chosen meshes. It is very interesting to observe that the solutions were converged from the mesh with 83×76 points.

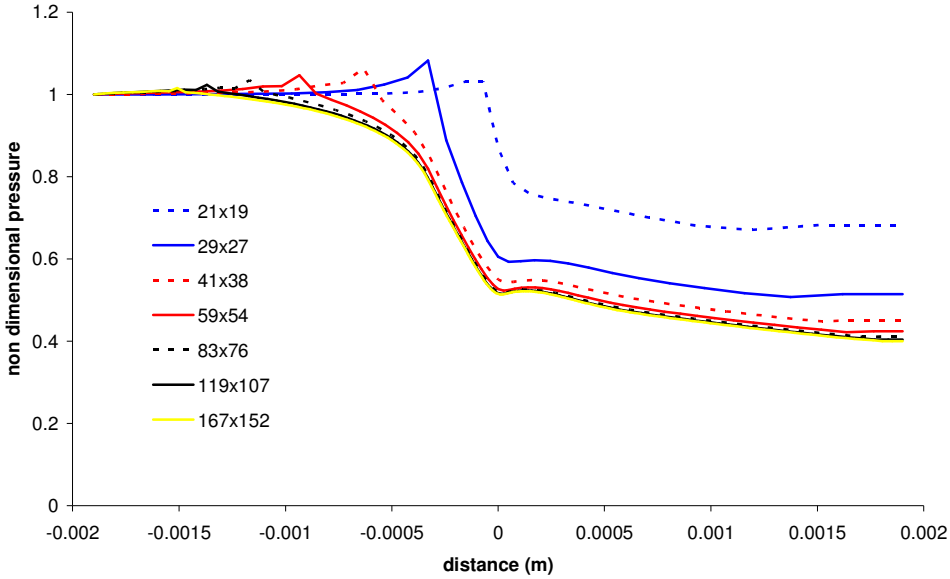

Figure 9. Pressure distribution in the lower wall of the convergent-divergent nozzle for seven meshes with progressive refinements.

4. CONCLUSION

It was presented the recent modifications made in an Euler code to account for laminar flow simulations. Verification and Validation procedures were also addressed as they are important tools to assure reliability of numerical

solutions. Five different physical problems were chosen to test the new code, confirming its reliability for each particular physical application: incompressible boundary-layer, compressible boundary-layer, shock-wave over compressible boundary-layer, Poiseuille flow, and convergent-divergent supersonic nozzle flow.

Some aspects concerning the Verification and Validation procedures were presented showing the importance of them for two physical solutions: in Poiseuille flow the order of the method was determined and in convergent-divergent supersonic nozzle flow a grid refinement was investigated.

Each physical problem was documented in such a way that allows them to be mimicked. Other similar solutions from the literature are also cited and, in some cases, they are compared with the present work results.

The numerical code showed good performance for all study cases analyzed. Good results were also obtained for low incompressible problems, as the laminar incompressible boundary-layer over a flat plate and flow between flat plates. The next step in the code development (turbulence model) can be now implemented aiming its use for the simulation in the Pilot Transonic Wind Tunnel of IAE.

5. REFERENCES

Anderson, D. A., Tannehill, J. C., Pletcher, R. H., 1984, "Computational Fluid Mechanics and Heat Transfer," Hemisphere Publishing Corp.

ASME Committee PTC-61, 2008, "ANSI Standard V&V 20 ASME Guide on Verification and Validation in Computational Fluid Dynamics and Heat Transfer", (submitted in 2009).

Beam, R. M., Warming, R. F., 1978, "An Implicit Factored Scheme for the Compressible Navier-Stokes Equations." AIAA Journal, Vol. 16, no. 4, pp. 393-402.

Blasius, H., 1950, "The Boundary Layers in Fluids with Little Friction," NACA TM 1256.

Cortell, R., 2005, "Numerical Solutions of the Classical Blasius Flat-Plate Problem," Applied Mathematics and Computation, Vol. 170, pp. 706-710.

Dolling, D. S., 2001, "Fifty Years of Shock-Wave/Boundary-Layer Interaction Research: What Next?," AIAA Journal, v. 39, n. 8, pp. 1517-1531.

Falcão Filho, J. B. P., 2006, "Estudo Numérico do Processo de Injeção em um Túnel de Vento Transônico", Dissertação de Doutorado, Instituto Tecnológico de Aeronáutica, São José dos Campos.

Falcão Filho, J. B. P., Ortega, M. A., 2008, "Numerical Study of the Injection Process in a Transonic Wind Tunnel. The Numerical Details," Computers and Fluids, Vol. 37, Issue 10, December 2008, pp. 1276-1308, available online in: www.sciencedirect.com. DOI: 10.1016/j.compfluid.2007.10.015.

Goffert, B., Falcão Filho, J. B. P., 2009, "Euler Equations Applied to Flow Over NACA 0012," 20th International Congress of Mechanical Engineering – COBEM, Gramado, RS.

König, B., Pätzold, M., Lutz, T., Krämer, E., Rosemann, H., Richter, K., Uhlemann, H., 2008, "Numerical and Experimental Validation of Three-Dimensional Shock Control Bumps," Anais do 4th Flow Control Conference of AIAA, Seattle, Washington.

MacCormack, R. W., 1981, "A numerical method for solving the equations of compressible viscous flow." St. Louis: AIAA paper 88-0110.

Mello, O. A. F., 1994, "An Improved Hybrid Navier-Stokes: Full-Potential Method for Computation of Unsteady Compressible Viscous Flows", PhD Dissertation, Georgia Institute of Technology, Atlanta.

Murman, E. M., 1972, "Computation of Wall Effects in Ventilated Transonic Wind Tunnels," AIAA paper, no. 72-1007, 7th Aerodynamic Testing Conference, Palo Alto.

Oberkampf, W. L., Trucano, T. G., 2002, "Verification and Validation in Computational Fluid Dynamics," Progress in Aerospace Sciences, Vol. 38, pp. 209-272.

Pulliam, T. H., 1986, "Artificial Dissipation Models for the Euler Equations", AIAA Journal, Vol. 24, nº12, pp. 1931-1940.

Pulliam, T. H., Chaussee, D. S., 1981, "A Diagonal Form of an Implicit Aproximate-Factorization Algorithm", Journal of Computational Physics, Vol. 39, pp. 347-363.

Resende, O. C., 2004, "The Evolution of the Aerodynamic Design Tools and Transport Aircraft Wings at Embraer," Jornal of the Brazilian Society of Mechanical Sciences and Engineering, Vol. XXVI, No. 4, pp. 379-390.Resende

Schilichting, H., 1979, "Boundary-Layer Theory," Seventh Edition, McGraw-Hill Book Company, 817 p.

Volpe, G., 1993, "Performance of Compressible Flow Codes at Low Mach Numbers," AIAA Journal, Vol. 31, n 1, pp. 49-56.

6. RESPONSIBILITY NOTICE

The authors are the only responsible for the printed material included in this paper.